Charge carrier scattering by defects in semiconductors

Vincenzo Lordi,* Paul Erhart, and Daniel Åberg
Lawrence Livermore National Laboratory, Livermore, California 94550, USA
(Received 9 April 2010; revised manuscript received 11 May 2010; published 4 June 2010)

A first-principles framework for calculating the rates of charge carrier scattering by defects in semiconductors is presented. First a quantitative formalism is outlined, followed by the development of an approximate relative formalism that allows rapid assessment of the effects of different defects on carrier transport in given materials. Representative results are presented that demonstrate the applicability of the relative formalism, which achieves a three to four orders of magnitude reduction in computational cost compared to the full quantitative calculation. The differences between the two formalisms are discussed in light of average carrier scattering by a defect, differences between electron and hole scattering, and variations of the scattering matrix elements throughout the Brillouin zone. Results and analysis are presented within the Born approximation for carrier scattering, which is applicable in the absence of strong interactions between scattering centers (i.e., the dilute limit). The theory as presented can be extended to interacting defects without modification if they can be represented as a set of unit defect clusters/complexes without long-range correlated interactions between them.

DOI: 10.1103/PhysRevB.81.235204 PACS number(s): 72.20.Dp, 71.15.Mb, 72.10.Bg, 72.10.Fk

I. INTRODUCTION

The effect of defects (e.g., dopants or impurities) on carrier transport in semiconductors is of paramount importance for many practical applications.[1,2] For example, one may be interested in selecting optimal dopants or codopants to manipulate conductivity while also controlling the impact on carrier mobility, or one may wish to identify the most detrimental impurities in a material for targeted purification efforts. A predictive understanding of how different defects and combinations of defects modify a material's transport properties is required to achieve such goals. Traditionally, much of the utility of semiconducting materials stems from the ability to use dopants to vary the conductivity of a material over a wide range.[1,2] The ability to also engineer carrier transport characteristics, such as mobility, alongside properties such as conductivity and band gap, is highly desirable for the realization of many electronic and optoelectronic devices. Optimal device performance often critically depends on the ability to understand and control the concentrations of assorted defects in a material resulting from highly sensitive growth and fabrication processes.

Here, we present a predictive theoretical framework to assess the effects of defects on carrier transport in semiconductors. The problem is examined from the point of view of scattering by defects, with the goal of establishing an accurate and efficient methodology for computational defect engineering, to enable the optimization of carrier transport concomitantly with other desired properties of a material. We present a quantitative formalism for evaluation of carrier scattering from first principles, then develop an approximate relative formalism which we show well-represents the relative behavior of different defects in a given material or similar materials with a significantly reduced computational cost. Illustrative results for a set of impurities in AlSb are used to compare different levels of approximation and to discuss differences in light of variations of the scattering matrix elements throughout the Brillouin zone as well as differences between electron and hole scattering. The theory as presented applies to the dilute defect limit or the limit of dispersed localized defect clusters (i.e., those that can be represented, for example, by a supercell model).

II. METHODS

A. Carrier scattering formalism

Defects perturb the electronic structure of an otherwise perfectly periodic crystal and act as scattering centers for electrons and holes traveling through the crystal. Fermi's Golden Rule can be used to obtain the rate of scattering of electrons from an initial state $|i\rangle$ into a final state $|f\rangle$ through a scattering potential ΔV as

$$R_{i\to f} = \frac{2\pi}{\hbar}|\langle f|\Delta V|i\rangle|^2 \delta(\varepsilon_i - \varepsilon_f), \tag{1}$$

where ε_i and ε_f are the energies of the initial and final states, respectively. The delta function indicates that the scattering is elastic. The use of Fermi's Golden Rule invokes the Born approximation, which implies that the scattering potential is treated as a perturbation (see further discussion in Sec. IV). To treat the scattering from first principles, the states and scattering potential are determined with an *ab initio* theory, such as density-functional theory (DFT) or beyond. Strictly, the scattering potential ΔV is the difference between the Hamiltonian operators of the ideal and the defect-containing system; however it is well approximated by the difference of the self-consistent local potentials between the defective and the ideal systems[3] (including both the electrostatic and exchange-correlation contributions, and full relaxation of the defect-containing system). Within first-order perturbation theory, the states $|i\rangle$ and $|f\rangle$ are taken from the unperturbed system.

The total scattering rate out of state $|i\rangle$, or equivalently the inverse lifetime of the state in the spirit of the relaxation time approximation for carrier transport, is obtained by summing over all possible final states for elastic scattering from state $|i\rangle$.[3,4] This summation amounts to an integration over the Brillouin zone via

$$\tilde{R}_{n\mathbf{k}} = \frac{1}{\tau_{n\mathbf{k}}} = c_{\mathrm{def}} \sum_{n'} \int \frac{d^3k'}{(2\pi)^3} R_{n\mathbf{k}\to n'\mathbf{k}'}(1-\cos\,\theta), \qquad (2)$$

where c_{def} is the density in the crystal of the defect under consideration (assuming a distribution of independent scattering centers), $|i\rangle = |n\mathbf{k}\rangle$ and $|f\rangle = |n'\mathbf{k}'\rangle$ have been written with explicit band (n) and k-point ($\mathbf{k}$) indices, and θ is the scattering angle (i.e., the angle between the group velocity vectors of the respective states, where the group velocity is obtained from the band structure via $\boldsymbol{v}_{n\mathbf{k}} = \frac{1}{\hbar}\nabla_{\mathbf{k}}\varepsilon_{n\mathbf{k}}$).[5]

The transport coefficients can then be obtained, for example, from the linearized Boltzmann equation by an additional Brillouin zone integration.[3,4] The result for the carrier mobility in a direction α for an applied electric field in the direction β is given by

$$\mu_{\alpha\beta} = -\frac{2e}{n_{\mathrm{carr}}} \sum_{n} \int \frac{d^3k}{(2\pi)^3} \tau_{n\mathbf{k}} (\boldsymbol{v}_{n\mathbf{k}} \cdot \hat{\alpha})(\boldsymbol{v}_{n\mathbf{k}} \cdot \hat{\beta}) \left.\frac{\partial f_0}{\partial \varepsilon}\right|_{\varepsilon_{n\mathbf{k}}}, \qquad (3)$$

where n_{carr} is the carrier concentration, $\tau_{n\mathbf{k}}$ is given by Eq. (2), f_0 is the Fermi distribution, and the factor of 2 accounts for spin (assuming non spin-polarized currents). The factor $\partial f_0/\partial\varepsilon$ in Eq. (3) indicates that only states near the band edge contribute significantly to the transport properties (i.e., only near the band edges do occupied initial states exist with appropriate available empty states into which to scatter).[6]

The calculation of Eq. (2) is quite computationally expensive, and the result converges slowly with the number of k points. To address this shortcoming, we developed an approximate form of the scattering strength which can be evaluated very rapidly. From inspection of the matrix elements in Eq. (1) and recognizing that the states $|i\rangle$ and $|f\rangle$ are always orthogonal (we are guaranteed that $|i\rangle \neq |f\rangle$ since a given state cannot scatter to itself), we observe that contributions to the matrix elements come only from regions in space where ΔV has a gradient; any DC component of ΔV will not affect the scattering rate. Therefore, we define a heuristic measure for the *relative carrier scattering strength* of a defect as

$$M = \int |\nabla_{\boldsymbol{r}}(\Delta V)| d\boldsymbol{r}, \qquad (4)$$

where M essentially measures the extent of the potential perturbation caused by the defect. Then, the *average scattering rate* will be approximately proportional to M^2. Since the approximate formalism in Eq. (4) does not incorporate information from the band structure, it does not distinguish between electron and hole scattering, as in Eqs. (2) and (3). Also, this approximate formalism can only be used to compare different systems insofar as the set of unperturbed wave functions that enter the matrix elements in Eq. (1) are equivalent or similar. Thus, the formalism of Eq. (4) may be used to compare defect carrier scattering in a given material or similar materials (for example, materials with identical or similar crystal structures). Care should be employed when comparing very different materials which may have qualitatively different unperturbed wave functions.

We have implemented both of the above formalisms within the projector augmented wave[8] (PAW) framework using the VASP code.[9–12] In the PAW formalism, the matrix elements in Eq. (1) have the form

$$\langle \psi_f | \Delta V | \psi_i \rangle = \langle \tilde{\psi}_f | \Delta V | \tilde{\psi}_i \rangle + \sum_{n,m} \langle \tilde{\psi}_f | \tilde{p}_n \rangle \hat{V}_{nm} \langle \tilde{p}_m | \tilde{\psi}_i \rangle, \qquad (5)$$

where

$$\hat{V}_{nm} = \langle \phi_n | \Delta V | \phi_m \rangle - \langle \tilde{\phi}_n | \Delta V | \tilde{\phi}_m \rangle. \qquad (6)$$

In Eq. (5), $|\tilde{\psi}\rangle$ indicates the "soft" plane-wave part of a wave function $|\psi\rangle$, and $|\tilde{p}_n\rangle$ are the PAW projector functions. In Eq. (6), $|\phi\rangle$ and $|\tilde{\phi}\rangle$ are the all-electron partial waves and pseudo partial waves, respectively, within the augmentation regions. Further details of these terms and the PAW method are found in Ref. 8. Because ΔV is local and confined within the supercell (see Sec. IV for further details), the spatial integrations need only be performed over a single supercell when done in real space.

We use the formalisms above to assess the effects of various defects and impurities on the transport properties of given materials. In this paper, the electron and hole mobilities will be used as an illustrative example. In principle, we at least need to calculate the average scattering rates given by Eq. (2) for all relevant states representing conducting channels at the operating temperature (e.g., for electrons, all states within $\sim 3\ k_B T$, or 78 meV at room temperature, of the bottom of the conduction band). Alternatively, the average scattering rates can be approximated using Eq. (4) with much less computational expense. A more accurate assessment would be based on the full calculation represented by Eq. (3), from which concentration-dependent electron and hole mobilities can be calculated for each defect or impurity under consideration, in order to compare them based on the actual concentrations of each impurity. The total mobility of a material containing multiple types of (noninteracting) defects is calculated by combining the separate results via $\mu_{\mathrm{total}}^{-1} = \Sigma_i \mu_i^{-1}$, where each μ_i is evaluated at the respective defect concentration $c_{\mathrm{def},i}$. We test and compare the applicability of each of these approaches in this paper.

B. Computational details

The calculations presented in this paper were conducted using density functional theory within the local density approximation (LDA), using the VASP code.[9–12] The calculations were performed with 64-atom cubic supercells of the zinc-blende structure of the test case material, AlSb. The LDA-relaxed lattice constant of 6.1213 Å was used.[13] The projector augmented wave method was used, with the energy cutoff for the plane-wave part of the wave functions set to 500 eV. The density of the FFT grid, and the corresponding real-space grid upon which the plane-wave part of the local potentials was defined, was typically $160\times160\times160$, or 4.5×10^{-4} Å^3 per grid point. Within the augmentation spheres, the grid density was doubled in each direction. Atomic relaxations were performed using a $6\times6\times6$ Monkhorst-Pack k-point mesh[14] until all forces were below

20 meV/Å. Gaussian smearing with a width of 0.1 eV was used for Brillouin zone integrations of the energy and forces. The evaluation of local potentials was performed with the same k-point grid and included the contributions from both the electrostatic terms and the exchange-correlation terms. For charged defect calculations, a homogeneous background charge was included (by omitting the $G=0$ term in the potential) to ensure charge neutrality of the entire cell.

C. Comments on computation

The root of the computational burden of Eq. (2) is that a brute-force evaluation of the integral requires a dense k point mesh throughout the entire Brillouin zone. The dense mesh is required to smoothly sample the complicated constant-energy elastic scattering isosurfaces in the three-dimensional reciprocal space, while accurately capturing variations of the scattering matrix elements as a function of $(n\mathbf{k},n'\mathbf{k}')$ (for example, as shown later in Fig. 2). The brute force integration can be simplified by pre-screening the band structure for the relevant conduction pockets (identifying the neighborhoods of band minima up to several k_BT) and restricting the computation to this subset of reciprocal space. This approach allows a finer sampling of the Brillouin zone in the regions that contribute significantly to the integral without wasting computational resources on a uniform sampling of the entire Brillouin zone. Alternatively, interpolation schemes can also be employed to improve convergence of the integral when only a coarse grid of k points is tractable. For example, linear interpolation of the matrix elements between computed points can be used, or a more sophisticated scheme based on Wannier function interpolation of the matrix elements can lead to improved results.[15–17] An approximate simplification of Eq. (2) is also possible by employing an effective mass approximation to replace the δ function in Eq. (1) with an analytical density of states and using a set of averaged constant matrix elements for each relevant conduction valley.[18] However, this last approach can miss features of the band structure affecting transport, and also detracts somewhat from a fully first-principles scheme by employing a parametrized model.

A comment is also in order regarding the construction of the ΔV perturbation potential. Since in practice we perform plane-wave DFT calculations for the ideal and perturbed systems and subtract the self-consistent potentials (defined on discrete grids) from the two calculations to obtain ΔV, care must be taken to ensure that no coordinate shift is introduced in the perturbed structure after atomic relaxation has been performed. Any shift of the center of mass of the "host" atoms surrounding the defect region relative to the center of mass of the ideal system will introduce regular oscillations in ΔV, which will accumulate in the calculation of the scattering matrix elements. We have systematically investigated the magnitude of this effect by taking as the perturbed system a perfect crystal with a shifted origin and calculating the scattering matrix elements for several scattering channels throughout the Brillouin zone. We find as an empirical rule of thumb that center of mass shifts as small as ~0.02 Å can contribute up to 0.1 eV or more (~25% or more) to the matrix elements. Any center of mass shift in the coordinates should be kept to $\ll$0.005 Å to avoid biasing the results. In practice, this is best achieved by fixing the positions of several atoms far from the defect during the relaxation. In the calculations presented here, the residual center of mass shift of the host atoms was always less than 10^{-6} Å.

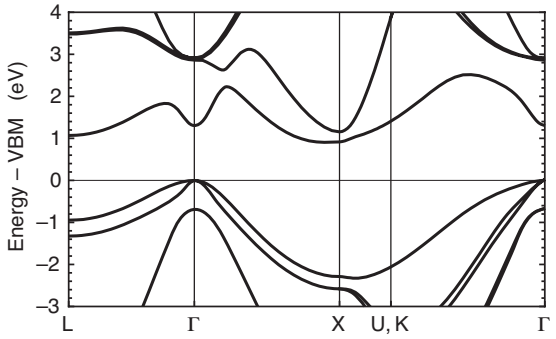

FIG. 1. Band structure for AlSb within the local density approximation. The valence band maximum (VBM) energy was set to zero.

III. RESULTS

We present results for a representative test case of a range of impurities in the zinc-blende semiconductor AlSb.[13,19] We have computed the values of the scattering matrix elements $\langle f|\Delta V|i\rangle$ for a variety of relevant scattering channels throughout the Brillouin zone and also the corresponding relative scattering rates M^2 from Eq. (4) for comparison. In addition, we have also performed the full calculations of Eqs. (2) and (3). We will show below that the approximate calculations using Eq. (4) very well reproduce the relative scattering rates found from the detailed calculations, while requiring 3 to 4 orders of magnitude less computing time.

To analyze the carrier scattering of different defects using the formalisms presented above, we first examine the band structure to determine the dominant conduction channels for electrons and holes. AlSb is an indirect band gap semiconductor, with the conduction band minimum at ~90% toward X from Γ and another minimum at the L point 160 meV higher (~6 k_BT at room temperature), as shown by the band structure in Fig. 1. The valence band maximum is at Γ, where the heavy hole (HH) and light hole (LH) bands are degenerate. The main conduction channel for electrons is in the X valley, with a minor contribution from the L valley that becomes more important as the temperature is elevated. Holes conduct through the HH and LH bands near Γ.

We have calculated the scattering matrix elements for various scattering channels within 2 k_BT of the conducting channel minima for electrons and holes, for various impurities in AlSb. The range of scattering channels considered span the three-dimensional space of the Brillouin zone. For example, for the X electron valley, there are scattering channels connecting nearby k points within the valley, as well as "g-type" [e.g., $(0,0,\xi)\rightarrow(0,0,-\xi)$] and "$f$-type" [e.g., $(0,0,\xi)\rightarrow(0,\xi,0)$] scattering channels. A similar set of scattering channels exists for the L valley. For holes, there are scattering channels both within and between the HH and LH bands.

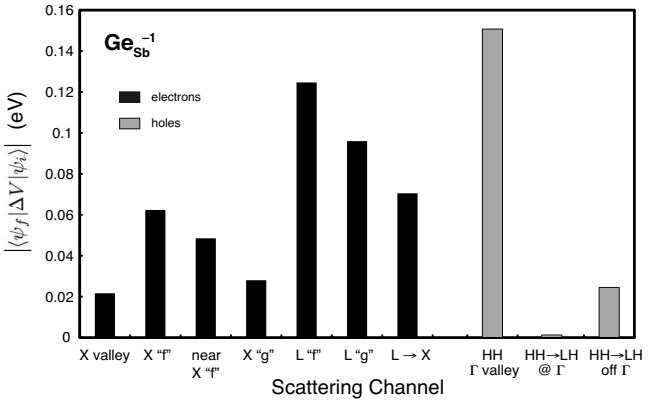

FIG. 2. Magnitude of the matrix element for selected scattering channels of electrons and holes for the Ge_{Sb}^{-1} impurity in AlSb. The direct reciprocal coordinates of the k points for the selected scattering channels are: X valley=$(0,0,0.84)\rightarrow(0,0,0.98)$, X "f"=$(0,0,0.9)\rightarrow(0,0.9,0)$, near X "f"=$(0,0,0.84)\rightarrow(0,0.98,0)$, X "g"=$(0,0,0.9)\rightarrow(0,0,-0.9)$, L "f"=$(0.5,0.5,0.5)\rightarrow(-0.5,0.5,0.5)$, L "g"=$(0.5,0.5,0.5)\rightarrow(-0.5,-0.5,-0.5)$, $L\rightarrow X$=$(0.5,0.5,0.5)\rightarrow(0,0,0.9)$, HH Γ valley=$(0.03,0.03,0.03)\rightarrow(0,0,0.02)$, HH→LH off Γ=$(0,0,0.04)\rightarrow(0,0,0.02)$. The electron scattering channels involve the lowest conduction band, for which the X valley minimum occurs at (0,0,0.9).

Figure 2 shows the variation of the magnitude of the scattering matrix element for selected electron and hole scattering channels for the Ge_{Sb}^{-1} impurity in AlSb, as an example. The specific k points involved in the selected transitions are given in the figure caption and represent the dominant elastic scattering channels near the respective band edges throughout the Brillouin zone. The most important electron scattering channel for low to moderate temperatures (e.g., room temperature) is around the conduction band minimum at the X valley, including f-type and g-type scatterings. Scattering that involves the L valley is stronger, but plays a significant role only at elevated temperatures. Hole scattering is seen to be dominated by heavy hole scattering at the Γ valence band maximum, with very little probability of scattering between heavy and light hole bands. Heavy hole and light hole states only couple away from Γ, where there is significant mixing of wave function character. Scattering of light holes is similar in magnitude to that of electrons, since the effective masses are similar. In general, hole scattering is stronger than electron scattering.

The Brillouin zone-averaged values of the scattering matrix elements for the whole set of impurities are shown in Figs. 3(a) and 3(b). The individual matrix elements for a given defect vary by up to 30% from the average between different channels. Within small neighborhoods of k-space, relatively smooth variations of the matrix elements were observed (see, for example, Fig. 2). The scattering rates in Figs. 3(a) and 3(b) are generally higher for holes than for electrons, indicating a lower hole mobility than electron mobility due to a higher hole effective mass compared to electrons. The difference between electrons and holes, however, is not very dramatic, which is consistent with empirical measurements of the hole mobility in this material being within about a factor of two of the measured electron mobility, for high quality material.[20–22]

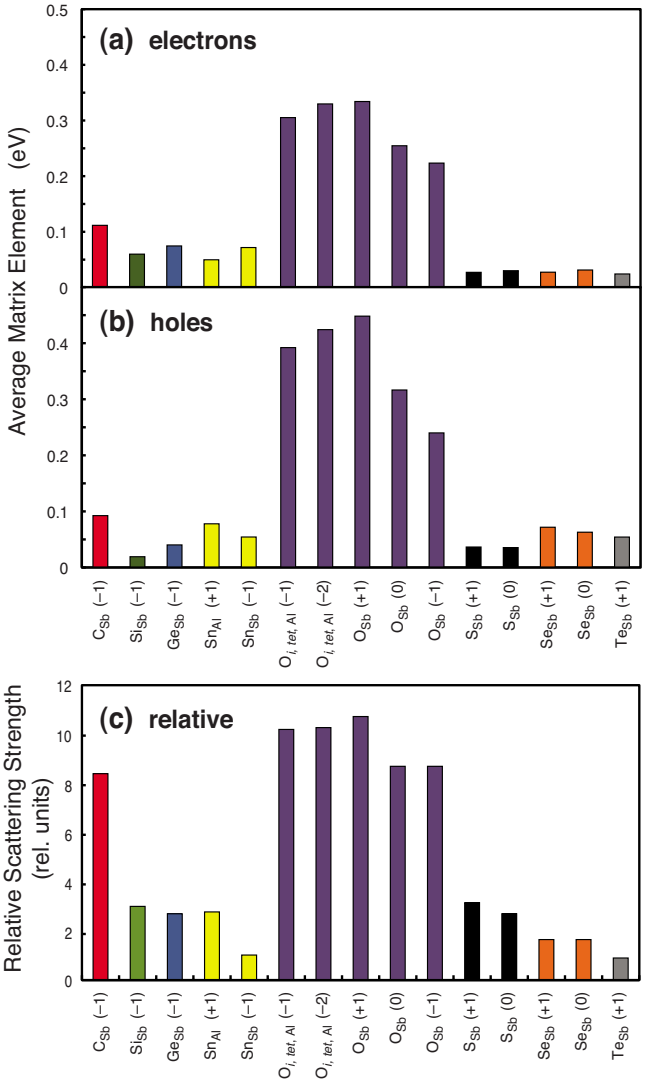

FIG. 3. (Color online) Magnitude of the scattering matrix elements averaged over the Brillouin zone for impurities in AlSb for (a) electrons and (b) holes. (c) Relative carrier scattering strengths, M, for impurities in AlSb calculated using Eq. (4). The values in (c) have been normalized by the value for Te_{Sb}^{+1}.

We can see from the average scattering rates in Figs. 3(a) and 3(b) that the different impurities scatter carriers by different amounts, and that the relative effects are essentially the same for electrons and holes. Oxygen by far is the strongest carrier scatterer, and carbon also is a notable scatterer, especially considering its typically high concentration in experimentally grown material. As a general rule, a substitutional impurity scatters less the larger its atomic radius, which is a result of the reduced size mismatch with Sb and consequently reduced lattice distortion. Oxygen is a very strong carrier scatterer because it not only has a small atomic radius, but also grossly distorts the lattice, predominantly entering either as an interstitial or a highly C_{3v}-distorted substitution.[19]

For comparison, Fig. 3(c) shows the approximate relative scattering strengths calculated via Eq. (4) for the same set of defects shown in Figs. 3(a) and 3(b). Comparing to Figs. 3(a) and 3(b), we see that the Eq. (4) results are reasonably pro-

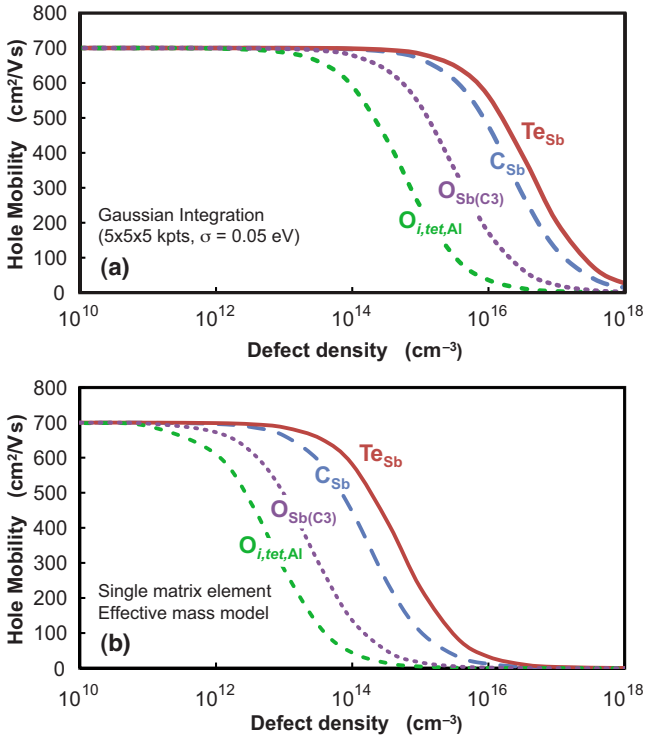

FIG. 4. (Color online) Calculated hole mobility at 300 K as a function of defect density for selected defects in AlSb, assuming only the defect of interest is present in each case. Charged defects are assumed to dope the material accordingly as the density is increased (C and O are acceptors, Te is a donor). In (a), Eqs. (1)–(3) are solved directly using a $5\times5\times5$ uniform k-point mesh and Gaussian smearing. In (b), an effective mass model using a single computed matrix element ($\mathcal{T}_{\mathrm{Te}}=0.0572$, $\mathcal{T}_{\mathrm{C}}=0.0955$, $\mathcal{T}_{\mathrm{O_{Sb}}}=0.258$, $\mathcal{T}_{\mathrm{O}_i}=0.489$ eV) and an analytical density of states based on the calculated band structure is used (see the Appendix). The phonon-limited mobility value at low densities was set at 700 $\mathrm{cm}^2/\mathrm{V\,s}$, based on a theoretical prediction using deformation potential scattering (Ref. 21).

portional to the average scattering rates calculated with the more detailed formalism. Therefore, the approximate formalism is useful for screening large numbers of defects rapidly to help categorize defects as mobility killers or benign impurities, without a large computational expense.

The average scattering rates are also compared to a full calculation of the mobility from Eqs. (1)–(3), shown in Fig. 4 for a select set of defects. In each case only the defect under consideration is assumed to be present in the material, to enable comparison of the relative effect of each defect on the mobility. The carrier density in the material is assumed to vary with the defect density, according to the doping characteristic (charge state) of each defect. The Fermi level corresponding to a given carrier density is obtained by numerical integration of the calculated density of states. We have set the phonon-limited mobility value at low-carrier densities to 700 $\mathrm{cm}^2/\mathrm{V\,s}$, based on a theoretical prediction using deformation potential scattering.[21] In Fig. 4(a), Eqs. (1)–(3) are evaluated directly, using a uniform k-point mesh to perform the Brillouin zone integrations. The results using a $5\times5\times5$ uniform k-point mesh of the supercell's Brillouin zone and Gaussian smearing of the delta function are shown to illustrate the convergence with k-point density for a uniform sampling of the Brillouin zone. Since the discrete sampling of the Brillouin zone underestimates $\tilde{R}_{n\mathbf{k}}$ of Eq. (2) by incompletely counting all contributions to the integral, the calculated mobility is overestimated before convergence with k-point density is achieved. For the case of hole mobility shown in Fig. 4, the scattering is confined to a single valley since the valence band structure exhibits a prominent maximum at the Γ point, and we can well approximate the converged result semianalytically using an effective mass approximation and a single, constant scattering matrix element (computed near the band maximum), since the matrix elements do not vary much within the scattering basin (the resulting formula for the mobility is derived in the Appendix). This semianalytical result is shown in Fig. 4(b), which may be regarded as an approximation of the fully converged calculation. We see that the coarsely sampled Brillouin zone integrations in Fig. 4(a) indeed overestimate the mobilities, but that otherwise the results are comparable. In fact, the final converged results lie in between these two limits since the semianalytical approach slightly underestimates the mobility in this case. Finally, comparison with Fig. 3 shows that the relative scattering strengths computed with Eq. (4) properly predict the impact on mobility of each defect.

IV. DISCUSSION

The utility and validity of the approximate relative formalism of Eq. (4), compared to the fully quantitative scheme represented by Eqs. (1) and (2), is demonstrated in the results presented above. The success of Eq. (4) in approximating the average scattering matrix element (on a relative scale) relates to its interpretation as a measure of the strength of the perturbation potential. This measure is valid only if the perturbation is sufficiently local. Particularly, the perturbation potential at least must fit within the calculation supercell and decay to zero sufficiently far from the cell boundaries. This requirement is related to the Born approximation, which enables the application of Fermi's Golden Rule to calculate scattering rates as long as the scattering potential may be validly regarded as a perturbation. The criteria which must be satisfied for the Born approximation to be valid are[23]

$$|U| \ll \frac{\hbar^2}{ma^2} \tag{7}$$

or

$$|U| \ll \frac{\hbar^2}{ma^2}ka, \tag{8}$$

where $|U|$ is the magnitude of the perturbing potential, a is the (order of magnitude) range of U, m is the reduced mass of the interacting particles (which, in the present context, is the carrier effective mass), and k is the magnitude of the wave vector. Either of Eqs. (7) and (8) may be satisfied, but Eq. (7) is more general. While Eq. (7) represents the usual interpretation that the perturbation potential must be small compared to the energy scale of interest, Eq. (8) indicates

that the Born approximation is also always valid for sufficiently fast particles when their energies are low compared to the perturbation.[24] A relationship is apparent between the criteria of Eqs. (7) and (8), where $|U|a$ is an approximate measure of the extent of the perturbation potential, and the relative scattering strength M of Eq. (4).

The criteria of Eqs. (7) and (8) can be used to verify the applicability of the theory described above for a particular case. These criteria must hold both for the relative formalism of Eq. (4) and for the full formalism of Eq. (1). In practice, for point defect-related scattering, the condition can almost always be met by considering a sufficiently large supercell, provided the density of defects is low enough that collective scattering does not dominate (typically less than $\sim 10^{18}-10^{19}$ cm^{-3}). In such a case, the perturbation potential is local and also sufficiently small compared to the energy of the free carriers (approximately the Fermi level).

The perturbative approach to carrier scattering employed here should not be extended to such high-defect concentration that individual defects can no longer be treated as independent scattering centers [violating the use of the n_{def} factor in Eq. (2)]. As a rule of thumb, defects begin to interact strongly at densities greater than at least 10^{19} cm^{-3}, which is much higher than the densities we consider in this work. A defect cluster (e.g., a complex) can be treated as a unit in a large supercell to capture the effects of local interactions between the constituent defects, so long as the total defect density is not so high that long-range correlation between scattering centers becomes significant. For very high-defect densities, bandlike transport associated with the defect network may become important as well and is not described by the perturbative scattering approximation presented here.

Furthermore, the results presented above relate predominantly to scattering induced by lattice strain from the defects, as demonstrated by the trends in the results for the substitutional impurities of different atomic radii (Fig. 3 and discussion above). The electrostatic effects of Coulomb scattering from charged defects is only included up to a range for which the dielectrically screened Coulomb potential fits within the supercell used in the calculations. Since the r^{-1} tail of the Coulomb potential is long ranged, the supercell only captures a portion of the total electrostatic interaction and the Coulomb scattering contribution is underestimated. However, in the context of the present discussion, we are mostly interested in a comparison of the scattering effects of different defects in a given material, for example in a search for optimal dopants. In this case, we are usually comparing defects with the same (absolute) charge state, for which the Coulomb scattering is identical. (Compare the charge states of the relevant impurities in AlSb shown in Fig. 3.) Therefore, we can still use the formalisms above to make comparative assessments of the relative scattering rates of different defects and impurities, despite the absolute underestimate of the Coulomb scattering. If necessary, one can account for the full Coulomb contribution to the scattering by simply extending the (screened) Coulomb potential for charged defects outside the supercell analytically, use Bloch's theorem to construct extended wave functions, and perform the calculation in an effectively larger supercell with only modest computational overhead.[25,26]

In addition, we have not explicitly included carrier scattering by phonons in our discussion, since the main interest of this work is defect engineering. Phonon scattering contributes a constant upper limit to the transport (see, for example, Fig. 4), essentially independent of (point) defect concentration.[26] For the typical range of defect concentrations that can be well-controlled experimentally ($c_{\mathrm{def}} \gtrsim 10^{14}$ cm^{-3}), impurity scattering comprises at least a considerable contribution to the total mobility, if not the dominant contribution.[26] From a practical perspective, the analysis of impurity scattering enables the identification of appropriate targets for material purification, in an attempt to approach the phonon limit. Nonetheless, if required, the phonon-limited contribution to the transport may be calculated and included, using either semiempirical[4,27–30] or *ab initio* methods.[26]

V. CONCLUSIONS

We have presented a first-principles framework for calculating the rates of charge carrier scattering by defects in semiconductors. From a quantitative formalism based on the Born approximation, we developed an approximate relative formalism which is significantly less expensive computationally. We showed good relative agreement between the approximate calculation and a full calculation. The relative formalism is particularly useful for rapidly assessing the relative effects of different defects or impurities on carrier transport in a given or similar material(s), and is suited for predictive calculations, particularly within density functional theory. The relative formalism, however, represents only average scattering and does not distinguish between electron and hole scattering or reveal the variation of scattering rate throughout the Brillouin zone. Results were presented for a representative test case of scattering from various impurities in AlSb. Evaluations of the scattering matrix elements throughout the Brillouin zone were presented to show typical variations with scattering vector and also to compare electron and hole scattering. The general theory presented is applicable in the dilute defect limit or in the limit of localized defect clusters that can be modeled as units without long-range correlated interactions between clusters.

ACKNOWLEDGMENTS

This work performed under the auspices of the U.S. Department of Energy by Lawrence Livermore National Laboratory under Contract DE-AC52-07NA27344, with support from the Laboratory Directed Research and Development Program and from the National Nuclear Security Administration Office of Nonproliferation Research and Development (NA-22).

APPENDIX: EFFECTIVE MASS MODEL IN A SINGLE SCATTERING VALLEY

For carrier transport dominated by scattering in a single valley, such as the case for hole transport in a semiconductor with a prominent Γ valence band maximum (no intervalley scattering possible), we may reasonably well describe the

transport using an effective mass approximation of the band structure. The Fermi occupation factor in Eq. (3) implies that only scattering very near the band edge will contribute to the mobility, so we may replace the energy- and wave vector-dependent scattering matrix element with a single constant value representative of the relevant intravalley scattering channel, and define

$$\mathcal{T} = \langle \psi_{f_0} | \Delta V | \psi_{i_0} \rangle \tag{A1}$$

as that constant matrix element, where the subscripts f_0 and i_0 indicate that a single pair of states is chosen near the bottom of the valley.

In the effective mass approximation, the parabolic band dispersion is given by

$$\varepsilon = \frac{\hbar^2 |k|^2}{2m^*}, \tag{A2}$$

where m^* is the density of states effective mass given by $m^* = (m_1^* m_2^* m_3^*)^{1/3}$ with m_i^* the effective mass in the ith principal direction. Thus,

$$|k|^2 = \frac{2m^* \varepsilon}{\hbar^2} \tag{A3}$$

and

$$d|k| = \frac{1}{\hbar} \sqrt{\frac{m^*}{2\varepsilon}} d\varepsilon, \tag{A4}$$

Changing variables from $d\mathbf{k}$ to $d\varepsilon$ for the integrals in Eqs. (2) and (3), for a parabolic band, gives

$$\int d\mathbf{k} \to 4\pi \int |k|^2 d|k|, \tag{A5}$$

$$= 4\pi \int \left(\frac{2m^* \varepsilon}{\hbar^2} \right) \frac{1}{\hbar} \sqrt{\frac{m^*}{2\varepsilon}} d\varepsilon, \tag{A6}$$

$$= \frac{4\sqrt{2}\pi}{\hbar^3} (m^*)^{3/2} \int \sqrt{\varepsilon} d\varepsilon, \tag{A7}$$

Then, plugging into Eqs. (2) and (3) and integrating over energy gives

$$\mu = \frac{8\pi^2 \hbar}{n_{\text{carr}} c_{\text{def}} \Omega^2 m^* \mathcal{T}^2} F^D(\varepsilon_F, T), \tag{A8}$$

with

$$F^D(\varepsilon_F, T) = \int_0^\infty \frac{\varepsilon}{2\ k_B T \left[1 + \cosh\left(\frac{\varepsilon - \varepsilon_F}{k_B T} \right) \right]} d\varepsilon. \tag{A9}$$

The upper integration limit in Eq. (A9) runs to ∞, but the integral converges rapidly by $\sim 10\ k_B T$. Here, Ω is the volume of the supercell.

*lordi2@llnl.gov

[1] R. F. Pierret, *Semiconductor Device Fundamentals* (Addison-Wesley, New York, 1996).
[2] P. Y. Yu and M. Cardona, *Fundamentals of Semiconductor Physics* (Springer-Verlag, New York, 1996).
[3] D. Chattopadhyay and H. J. Queisser, Rev. Mod. Phys. **53**, 745 (1981).
[4] M. V. Fischetti and S. E. Laux, J. Appl. Phys. **80**, 2234 (1996).
[5] M. H. Evans *et al.*, Phys. Rev. Lett. **95**, 106802 (2005).
[6] We note that the use of the Boltzmann transport equation in obtaining Eq. (3) invalidates its use at very high electric fields, very high carrier energies, or for carriers with very short lifetimes (Ref. 7). Furthermore, Eq. (3) is only valid for the homogeneous, steady-state response to a time-independent electric field (Ref. 3).
[7] M. V. Fischetti and S. E. Laux, Phys. Rev. B **38**, 9721 (1988).
[8] P. E. Blöchl, Phys. Rev. B **50**, 17953 (1994).
[9] G. Kresse and J. Hafner, Phys. Rev. B **47**, 558 (1993).
[10] G. Kresse and J. Hafner, Phys. Rev. B **49**, 14251 (1994).
[11] G. Kresse and J. Furthmüller, Phys. Rev. B **54**, 11169 (1996).
[12] G. Kresse and J. Furthmüller, Comput. Mater. Sci. **6**, 15 (1996).
[13] D. Åberg, P. Erhart, A. J. Williamson, and V. Lordi, Phys. Rev. B **77**, 165206 (2008).
[14] H. J. Monkhorst and J. D. Pack, Phys. Rev. B **13**, 5188 (1976).
[15] F. Giustino, Jonathan R. Yates, I. Souza, M. L. Cohen, and S. G. Louie, Phys. Rev. Lett. **98**, 047005 (2007).
[16] N. Marzari and D. Vanderbilt, Phys. Rev. B **56**, 12847 (1997).
[17] I. Souza, N. Marzari, and D. Vanderbilt, Phys. Rev. B **65**, 035109 (2001).
[18] F. Murphy-Armando and S. Fahy, Phys. Rev. Lett. **97**, 096606 (2006).
[19] P. Erhart, D. Åberg, and V. Lordi, Phys. Rev. B **81**, 195216 (2010).
[20] W. P. Allred *et al.*, J. Electrochem. Soc. **107**, 117 (1960).
[21] J. H. Yee, S. P. Swierkowski, and J. W. Sherohman, IEEE Trans. Nucl. Sci. **24**, 1962 (1977).
[22] K.-J. J. Wu (private communication).
[23] L. D. Landau and E. M. Lifshitz, *Quantum Mechanics (Non-Relativistic Theory)* (Pergamon Press, New York, 1977), p. 32.
[24] Equation (8) is satisfied for sufficiently fast particles whose energies are also sufficiently low, since the particle energy scales as $\frac{\hbar^2}{ma^2}(ka)^2$ (within the free-electron approximation).
[25] R. Rurali, T. Markussen, J. Suñé, M. Brandbyge, and A.-P. Jauho, Nano Lett. **8**, 2825 (2008).
[26] O. D. Restrepo, K. Varga, and S. T. Pantelides, Appl. Phys. Lett. **94**, 212103 (2009).
[27] C. G. Van de Walle and R. M. Martin, Phys. Rev. Lett. **62**, 2028 (1989).
[28] K. Seeger, *Semiconductor Physics*, 9th ed. (Springer, New York, 2004), Chap. 6.
[29] J. Bude, in *Monte Carlo Device Simulation: Full Band and Beyond*, edited by K. Hess (Kluwer, Norwell, MA, 1991), Chap. 2.
[30] J. R. Meyer and F. J. Bartoli, Phys. Rev. B **23**, 5413 (1981).